NEW TECHNOLOGIES WITH CONCRETE BLOCKS FOR TSUNAMI PROTECTION AND LONG-PERIOD WAVE ABSORPTION

by

Shin-ichi Kubota[1], Jun Mitsui[2], Masashi Tanaka[3] and Akira Matsumoto[2]

ABSTRACT

In Recent years, tsunami and long-period waves have caused problems in Japan. Numerous breakwaters were seriously damaged by the 2011 Off the Pacific Coast of Tohoku Earthquake Tsunami. Many ports suffered disturbance in cargo handling due to ship motion caused by long-period waves. This paper presents our new methods using concrete blocks for tsunami protection and long-period wave absorption as countermeasures to such problems. A simple and highly accurate stability estimation method for concrete blocks covering the rubble mound of a breakwater against tsunami overflow is proposed. In this method, the overflow depth is used to represent the external force. This enables an easier and more robust estimation of the required mass of the concrete blocks over that of the conventional method based on flow velocity. A submerged mound type long-period wave absorbing structure is proposed. It becomes clear that submerged structures display a higher wave absorbing performance compared with those of conventional structures.

1. INTRODUCTION

In recent years, among the various types of coastal structures, concrete blocks have gained wider use as one of the important components due to their effectiveness against wind wave attacks. The design method for wind waves is well established and concrete blocks work best. On the other hand, tsunami and long-period waves also cause problems in Japan. For many decades, tsunami protection for facilities has been studied. However, the 2011 Off the Pacific Coast of Tohoku Earthquake Tsunami which was beyond the scope of assumption damaged numerous breakwaters and new problems have emerged. Meanwhile, many ports suffer from disturbances in cargo handling due to ship motion caused by long-period waves. In this paper, we introduce some new methods using concrete blocks for tsunami protection and long-period wave absorption as countermeasures to such problems.

In the 2011 Off the Pacific Coast of Tohoku Earthquake Tsunami, one of the causes of failure of breakwaters subjected to tsunami attack was a scouring of the rubble foundation and subsoil on the harbor-side of the breakwater. This was previously inconceivable as a type of failure (Ministry of Land, Infrastructure, Transport and Tourism, 2013). One possible countermeasure is placement of widened protection using additional rubble stones behind the breakwater to prevent sliding of the caisson. Placing concrete blocks on the widened protection would also be required to prevent the scouring around the rubble mound (Fig. 1). The Isbash formula (Coastal Engineering Research Center, 1977) has been applied previously as the method to estimate the required mass of concrete blocks against tsunami. The required mass calculated by this formula is proportional to the sixth power of the flow velocity near the armor unit. This causes the practical problem that the required mass is too sensitive to variations in the estimated flow velocity. In this context, the establishment of a more practical method to determine the mass of concrete blocks is one urgent issue towards the achievement of resilient breakwaters against tsunamis. Hydraulic model experiments in a wide range of conditions were conducted to extract key factors for concrete block stability by using a wave flume equipped with tsunami generator. Based on the experimental study, a new stability estimation method for concrete blocks placed on widened protection against tsunami overflow is proposed. The stability of the concrete blocks is estimated using an overflow depth of tsunami instead of flow velocity.

---

[1] FUDO TETRA CORPORATION, Technical Research Institute, shinichi.kubota@fudotetra.co.jp
[2] FUDO TETRA CORPORATION, Technical Research Institute
[3] FUDO TETRA CORPORATION, Civil Engineering Division

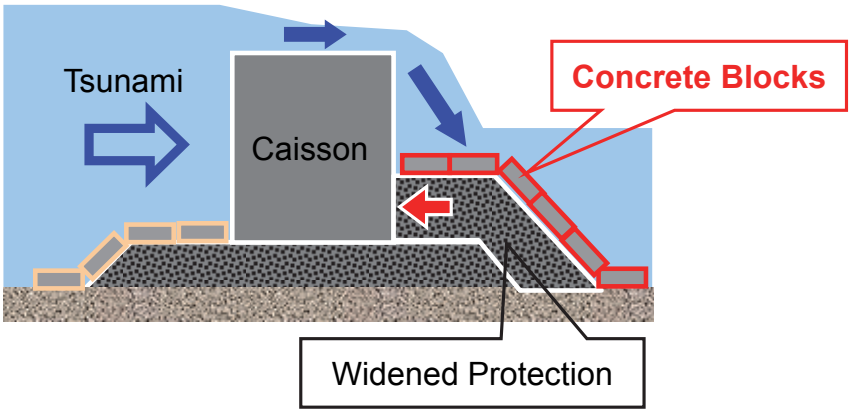

Figure 1: Countermeasure against Tsunami of Breakwaters

On the other hands, it has been reported that long-period waves with period of 30 to 200 s cause serious problems in cargo handling in many Japanese ports. The problems in cargo handling are mainly related to large motions on moored vessels which are caused by resonance with long-period waves in a harbor. As a countermeasure, wave absorbing mounds installed on the harbor side of breakwaters have been proposed and constructed. The crown heights of the rubble mounds are almost equal to those of the caissons. However, because of the poor wave absorbing performance of such conventional structures, the required mound width at the still water level for long-period waves becomes more than 30 m. It is important to reduce the size of the structure to apply to specific site condition. In this study, a submerged mound type long-period wave absorbing structure with high performance is proposed (Fig. 2). The basic concept of this proposed structure is to level the crest elevation to the water surface to establish high efficiency in energy dissipation on the surface of the crown of the concrete blocks. A series of hydraulic model experiments were carried out to evaluate the wave absorbing performance. The wave absorbing mechanism was investigated using hydraulic model experiments and numerical analyses.

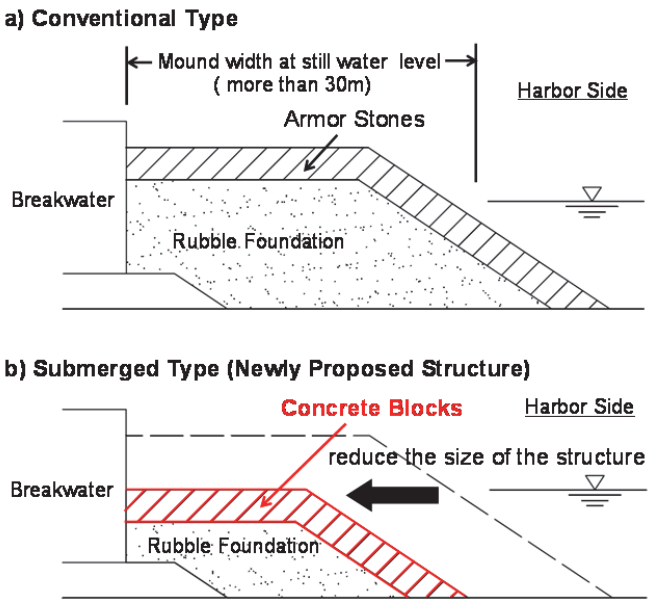

Figure 2: Long-period Wave Absorbing Structure

2. NEW TECHNOLOGY FOR TSUNAMI PROTECTION USING CONCRETE BLOCKS

2.1 Wave Flume Equipped with Tsunami Generator

A tsunami generating facility which consists of a circulating pump and a vacuum chamber has been installed in our wave flume (Fig.3). This tsunami generator can create various types of tsunami, such as steady flow which continuously overflow breakwaters and bores having steep wave fronts. A piston-type wavemaker is also available. It is possible to use this in combination with the circulating pump and the vacuum chamber. Hence, it will make possible to conduct wide-ranging studies of tsunami measures.

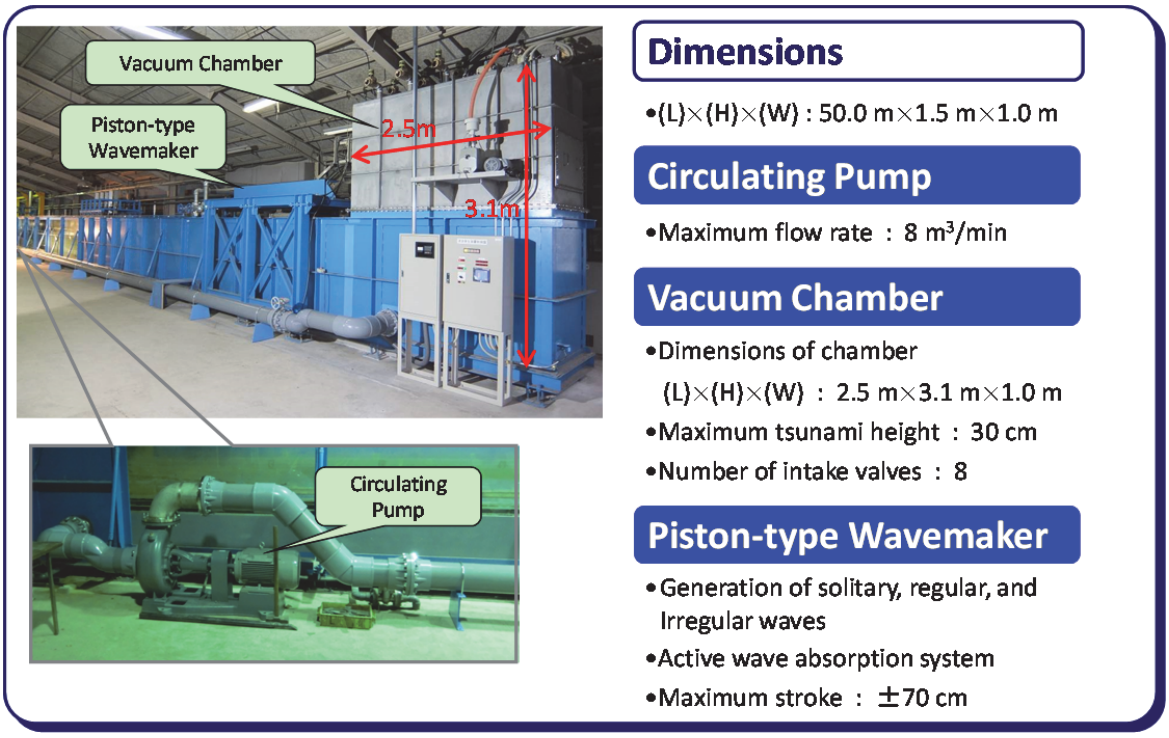

Figure 3: Overview of Tsunami Generator

2.2 Experimental Setup

Experiments were carried out in a 50 m long, 1.0 m wide, and 1.5 m deep wave flume equipped with the tsunami generator shown in Fig. 3. Fig. 4 shows test setup in the flume. A horizontal mortar seabed was partitioned into two sections along the length, and a breakwater model was installed in one 50 cm wide waterway. A submersible pump and discharge port were located on the harbor-side and sea-side of the breakwater model respectively to generate a steady overflow. A water level difference was generated between the inside and outside of the breakwater by operating the pump. The height of the sea-side water level could be changed by varying the height of the overflow weir installed on the sea-side of the breakwater model. The height of the overflow weir could be varied in a range of 0 to 50 cm. A vent hole with diameter of about 25 mm was provided in the partition wall close behind the caisson to maintain the space between the caisson and overflow nappe in ambient atmospheric pressure conditions.

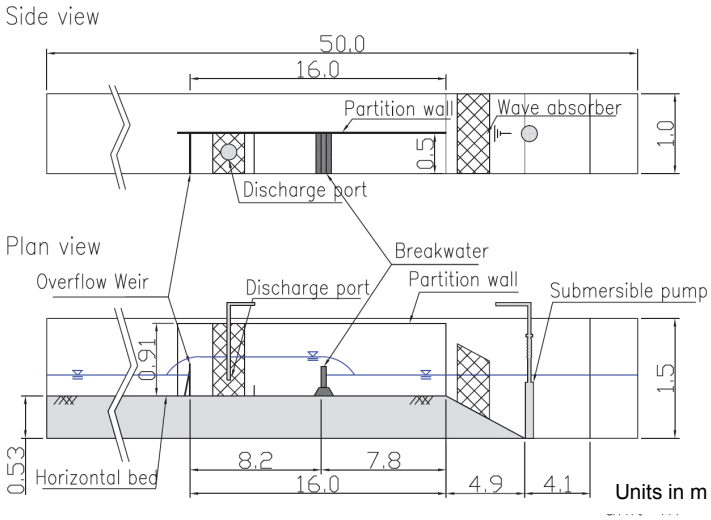

Figure 4: Test Setup in the Flume

A schematic layout of the breakwater model is shown in Fig. 5. The model scale is 1/50. Experiments were carried out by changing the shape of the harbor-side rubble mound, the harbor-side water level, and the shape and mass of the concrete blocks. Two kinds of flat-type blocks and a wave-dissipating block were used in the experiments as shown in Fig. 6. The flat-type block with five holes is a recently developed block named “Permex” produced by refining the “X-block” which has been used conventionally. The large holes in the block have been found to contribute to high stability against wave action due to the reduction of the uplift force (Hamaguchi et al. 2007, Kubota et al. 2008). The caisson model was made of wood and was fixed with a weight so that it would not be moved by tsunami action since this study was focused on the stability of concrete blocks.

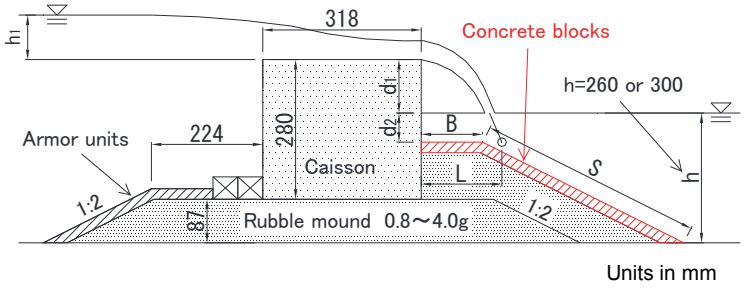

Figure 5: Schematic Layout of the Tested Breakwater

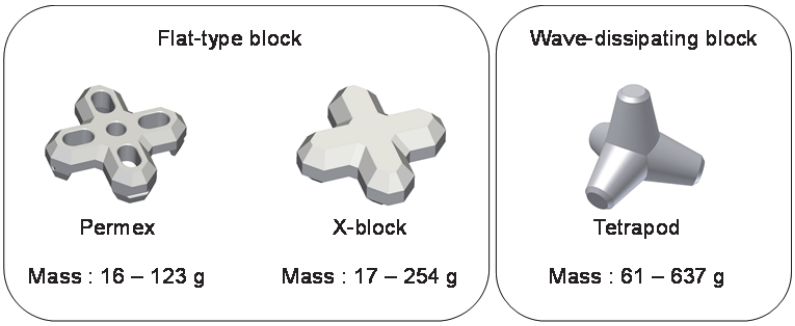

Figure 6: Concrete Blocks Used in the Experiment

The duration time of the steady overflow of tsunami was set to 127 s (15 min in the prototype scale) to simulate the actual event observed in Hachinohe port during the Tohoku tsunami on March, 11th in 2011. As it took about 60 s until the water level achieved a steady state from the start of operating the pump, the total operation time of the pump was set to 187 s. The stability limits of the armor units were examined by increasing the overflow depth in increments of 1 cm. The overflow depth was defined as the difference between the sea-side water level (measured at 2 m on the offshore side from the front of the caisson) and the crest height of the caisson. The harbor-side water level was measured at 2 m on the onshore side from the rear wall of the caisson. The section was not rebuilt after tsunami attack with each overflow depth. The number of the moved concrete blocks was counted as an accumulated number. The damage to concrete blocks were defined using the relative damage N_0, which is the actual number of displaced blocks related to the width of one nominal diameter D_n (Van der Meer 1988). The nominal diameter D_n is the cube root of the volume of the armor unit. In this study, N_0=0.3 was applied as the criterion of damage.

2.3 Feature of the Damage by Tsunami Overflow

Fig. 7 shows snapshots of the tsunami overflow in the experiment. As soon as the concrete blocks at the slope section were washed away, the scouring of the rubble mound progressed rapidly and reached to the sea bottom within about 1 minute (7 minutes in the prototype scale). Though widened protection using additional stones exhibits a function to delay scouring, the damage expands rapidly if the armor units are washed away and the rubble mound is exposed. This is one of the features of damage by tsunami overflow.

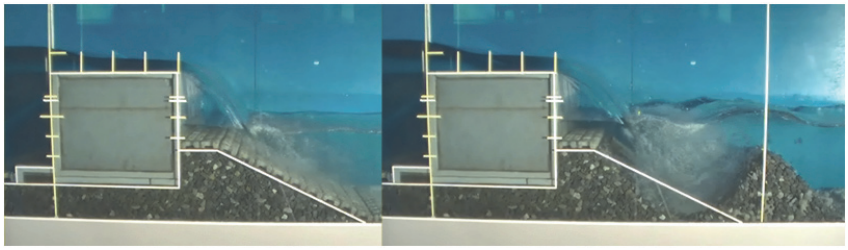

Figure 7: Snapshots of Tsunami Overflow

2.4 Influence of Impingement Position of Overflow Jet

The impingement position of the overflow jet will change with various factors such as the shape of the harbor-side mound and the overflow depth. The influence of the impingement position on block stability was examined by changing the crown width of the harbor-side mound. Fig. 8(a) shows an example of the stability test results. In this condition, the overflow jet impinged on the slope section when the number of armor units on the crown section was one or two, whereas it impinged on the crown section in the case of more than four units on the crown section. The cases in which the jet impinged on the slope section showed higher stability than the cases of impingement on the crown section. This shows that impingement position largely affects the block stability. Because the effect of the impingement position depended on the structural conditions such as the shape of the concrete block and the presence or absence of widened protection, it is necessary to incorporate properly this effect into the estimation of the block stability.

2.5 Influence of Harbor-side Water Level

When a tsunami overflows the caisson, the discharged water from the rear end of the caisson accelerates during the freefall above the water surface, and decelerates under the water surface due to diffusion. Therefore, the stability of concrete blocks should decrease as the crown height of the caisson above the harbor-side water level increases. Also, it should increase as the submerged depth above the concrete blocks increases. Fig. 8(b) shows a comparison of the stability test results with two different harbor-side water levels. On the whole, the results of deep-water cases showed higher stability than those of shallow-water cases.

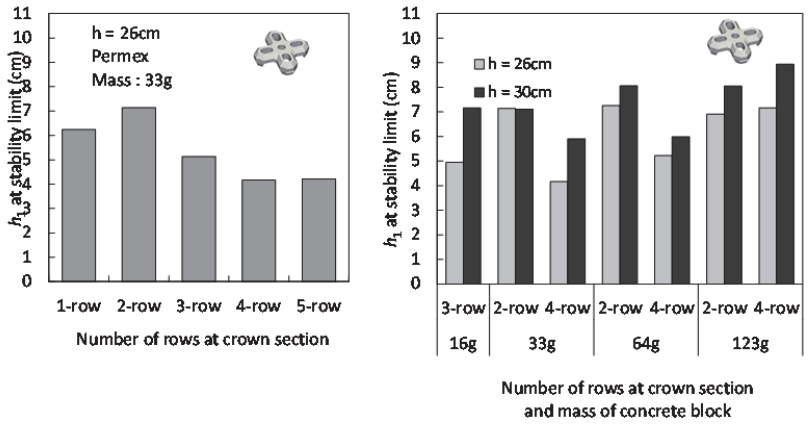

(a) Influence of Impingement Position **(b) Influence of Harbor-side Water Level**

Figure 8: Influence of Impingement Position and Harbor-side Water Level on the Overflow Depth h_1 at Stability Limit

2.6 Failure Modes of Concrete Blocks

Two failure modes for flat-type blocks were observed in the experiments. One was an overturning mode in which the concrete blocks near the impingement position overturned. The other was a sliding mode in which all the blocks on the slope section slid together. Fig. 9 shows the relationship between the nominal diameter of the concrete block D_n and the overflow depth h_1 on the occurrence of damage. In the cases of overturning mode, the overflow depth at the occurrence of damage was almost proportional to the nominal diameter D_n. On the other hand, in the cases of sliding mode, it had only a small dependence on D_n. These results suggest that enlargement of the block size causes an increase in the acting force as much as the increase in the resistance force with regard to the sliding mode. For the wave-dissipating blocks, almost every failure pattern was that of blocks near the impingement position being displaced individually.

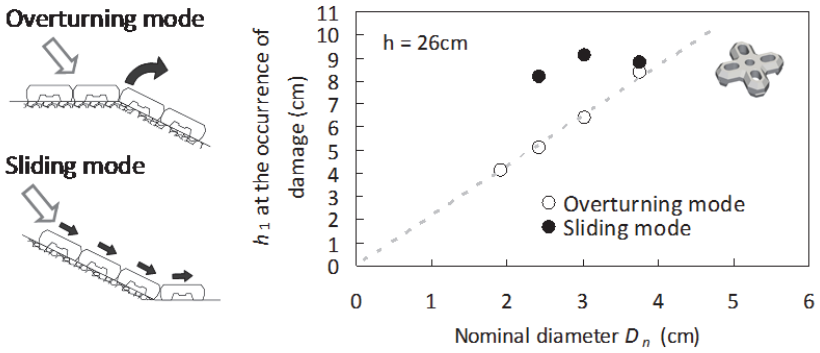

Figure 9: Relationship between the Nominal Diameter D_n and the Overflow Depth h_1 at the Occurrence of Damage by Each Failure Mode

2.7 Performance of the Wave-dissipating Concrete Blocks

A characteristic of the wave-dissipating blocks installed in two layers is that scouring becomes hard to progress rapidly even when many blocks are displaced. The reasons are considered to be the following:

(1) it takes a longer time before the rubble stones are exposed since they are covered with the two layers, (2) displaced blocks piled up behind the impingement position prevent the progress of the scouring by staying interlocked without being washed away. Avoiding the rapid progress of scouring is important from the viewpoint of resilience of a breakwater in the prevention of large scattering of the caisson (Arikawa et al. 2013). The widened protection mound covered with wave-dissipating blocks may provide such resilience.

2.8 Stability Estimation Method

Two empirical formulae for the stability estimation were derived based on the experimental results mentioned above. The overflow depth was used in the formulae to represent the external force. The overflow depth of the stability limit corresponding to each failure mode was obtained by the two formulae. The final stability limit was determined by the severer one. The formulae for the overturning mode and sliding mode are expressed as follows:

Overturning mode :
$$\frac{h_1}{(S_r-1)D_n} = N_{S1} = f\left(\frac{B}{L}, \frac{d_2}{d_1}\right) \tag{1}$$

Sliding mode :
$$\frac{h_1}{(S_r-1)S} = N_{S2} = f\left(\frac{d_2}{d_1}\right) \quad \text{for} \quad \frac{B}{L} \le 1.1 \tag{2}$$

where, h_1 is the overflow depth, S_r is the specific gravity of concrete with respect to seawater, S is the slope length of the harbor-side rubble mound, N_{S1} and N_{S2} are the stability numbers, B is the crown width of the harbor-side mound, L is the impingement position of the overflow jet, d_1 is the crown height of the caisson above the harbor-side water level, and d_2 is the submerged depth above the armor units (regarding the definition of symbols, see Fig. 5). Stability numbers N_{S1} and N_{S2} are functions of B/L and d_2/d_1, which are the parameters representing the influence of the impingement position and the harbor-side water level respectively. The stability is determined only by Eq. (1) if B/L is larger than 1.1 since failure by sliding mode does not occur when the overflow jet impinges on the crown section. Similarly, the stability of wave-dissipating blocks is also determined only by Eq. (1).

For the overturning mode, the overflow depth h_1 represents the acting force on armor units, whereas the nominal diameter of concrete blocks D_n represents the resistance force as shown in Eq. (1). For the sliding mode, on the other hand, the slope length S is used to represent the resistance force as shown in Eq. (2). This is because the resistance force should be represented by the total length of the blocks on the slope as the whole blocks on the slope section slide together in the sliding mode. As a result, the overflow depth of the stability limit in the sliding mode is not dependent on the block size as can be seen from Eq. (2). This corresponds with the experimental results described above (see Fig. 9).

2.9 Calculation Method of the Impingement Position

It is necessary to calculate the impingement position L to apply the estimation method. It can be calculated approximately using the overflow depth h_1 as shown below. The definition of each symbol is shown in Fig. 10.

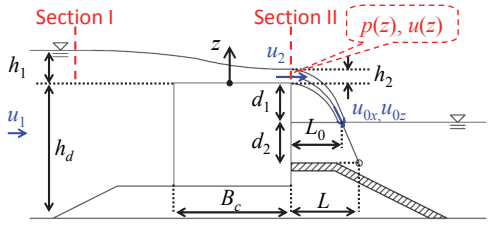

Figure 10: Definition of the symbols used in the calculation of the impingement position

The overflow discharge per unit width q is calculated by using the Hom-ma formula (Hom-ma 1940b):

$$q = 0.35h_1\sqrt{2gh_1} \tag{3}$$

where g is the acceleration due to gravity. The application condition in this formula is $h_1/B_c < 1/2$. The effect of the approaching velocity u_1 can be disregarded if $h_1/h_d < 0.5$ (Hom-ma 1940a). The water depth above the caisson at the rear end of the caisson h_2 and the cross sectional averaged flow velocity u_2 are calculated according to Hom-ma (1940a) as shown below.

Applying the Bernoulli's theorem to Sections I and II yields the following relation:

$$h_1 = z + \frac{p_{(z)}}{\rho g} + \frac{u_{(z)}^2}{2g} \tag{4}$$

where, z is the height measured from the top of the caisson, and $p_{(z)}$, $u_{(z)}$ are the pressure and the flow velocity at Section II, respectively. The overflow discharge q is obtained by integrating the flow velocity $u_{(z)}$ as follows:

$$q = \int_0^{h_2} \sqrt{2g\left(h_1 - z - \frac{p_{(z)}}{\rho g}\right)}dz \tag{5}$$

If the pressure distribution $p_{(z)}$ is obtained, h_2 can be calculated using Eq. (3) and Eq. (5). The pressure distributions were assumed as the following triangle distributions:

$$\begin{aligned} p_{(z)} &= \rho g\left(h_2 - z\right) \quad \text{for} \quad h_2/2 \le z \le h_2 \\ p_{(z)} &= \rho g z \quad \text{for} \quad 0 \le z \le h_2/2 \end{aligned} \tag{6}$$

Using Eq. (3), Eq. (5), and Eq. (6), one obtains Eq. (7):

$$0.35h_1\sqrt{2gh_1} = \sqrt{2g}\left\{-\frac{1}{3}\left[\sqrt{\left(h_1 - h_2\right)^3} - \sqrt{h_1^3}\right] + \sqrt{h_1 - h_2}\,\frac{h_2}{2}\right\} \tag{7}$$

The relationship between h_1 and h_2 are solved numerically with Newton's method as follows:

$$h_2 = 0.42h_1 \tag{8}$$

In this study, the following relationship was used considering its suitability to the experimental results:

$$h_2 = 0.45h_1 \tag{9}$$

The center of trajectory of the overflow water was then obtained under the following assumptions. The overflow water discharges horizontally from the rear end of the caisson at the flow velocity $u_2 = q/h_2$. The trajectory of the overflow nappe above the water surface is a parabola. The trajectory of the water below the water surface is a straight line.

The landing position of the overtflow water on the harbor-side water surface, L_0, and the flow velocity u_{0x}, u_{0z} are calculated as follows:

$$L_0 = u_2\sqrt{\frac{2\left(d_1 + h_2/2\right)}{g}} \tag{10}$$

$$u_{0x} = u_2, \quad u_{0z} = \sqrt{2g\left(d_1 + h_2/2\right)} \tag{11}$$

The impingement position L was thus obtained as follows:

$$L = L_0 + \frac{u_{0x}}{u_{0z}} d_2 \tag{12}$$

The stability numbers N_{S1} and N_{S2} are determined by applying the impingement position L calculated in this manner.

2.10 Determination of Stability Numbers

Fig. 11(a) shows the influence of the impingement position by plotting the stability number N_{S1} against B/L. The conditions of water depth are almost at the same level (d_2/d_1 = 0.47 to 0.66). The damage data with sliding mode is excluded in the figure to reveal the stability limit of overturning mode. The stability limit is expressed in a single line as a function of B/L regardless of the mass of the block. Also, the difference in the stability due to the impingement position appears clearly. Fig. 11(b) shows the influence of the harbor-side water depth by plotting the N_{S1} against d_2/d_1. The data on the conditions of B/L > 1.0 is used. The stability tends to increase as d_2/d_1 increases.

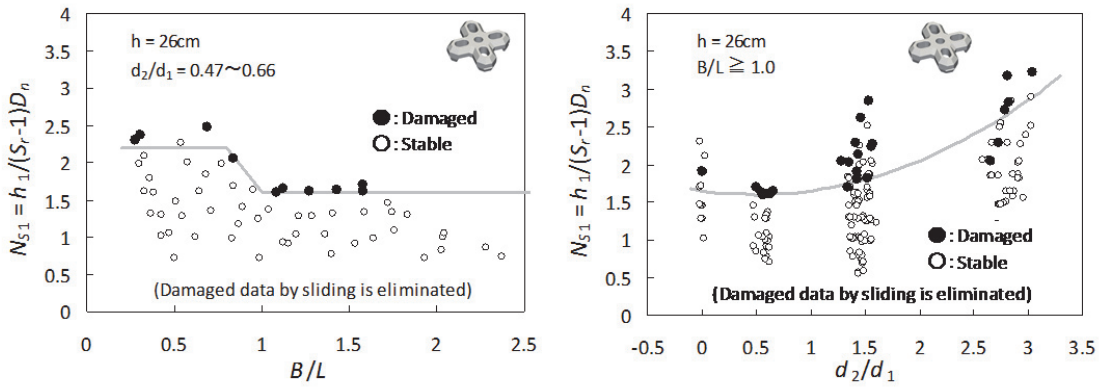

(a) Influence of B/L on N_{s1} **(b) Influence of d_2/d_1 on N_{s1}**

Figure 11: Influence of B/L and d_2/d_1 on N_{S1}

Fig. 12 shows the stability numbers N_{S1} and N_{S2} for flat-type blocks determined through all the test results. Different lines are used according to the B/L in Fig. 12(a). When B/L is between 0.8 and 1.0, the value is obtained by linear interpolation. The stability of the Permex is higher than that of the X-block for both failure modes. The stability number for the wave-dissipating block is shown in Fig. 13. In the case of the wave-dissipating block, the influence of the impingement position was different from the case of the flat-type blocks. Namely, the cases in which the jet impinged on the crown section showed higher stability than the cases of impingement on the slope section. This result was reflected in Fig. 13.

Fig. 14 shows a comparison of the estimated overflow depth of stability limit with the damaged overflow depth in the experiments. The estimated results are on the safe side as a whole, and they show good agreement for both failure modes.

The estimation method mentioned above is referred in the design guideline of breakwaters against tsunami (Ministry of Land, Infrastructure, Transport and Tourism, 2013) and is used for actual design.

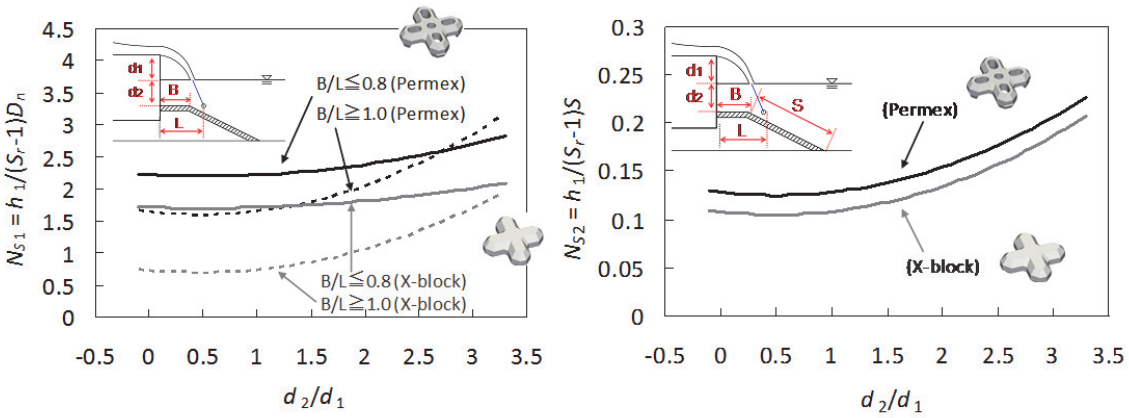

Figure 12: Stability Numbers for Flat-type Concrete Blocks

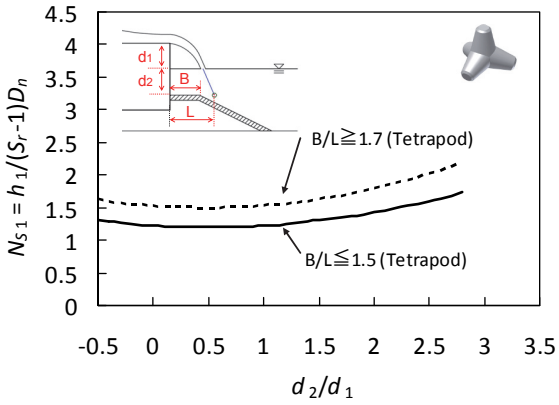

Figure 13: Stability Numbers for Wave-dissipating Concrete Blocks

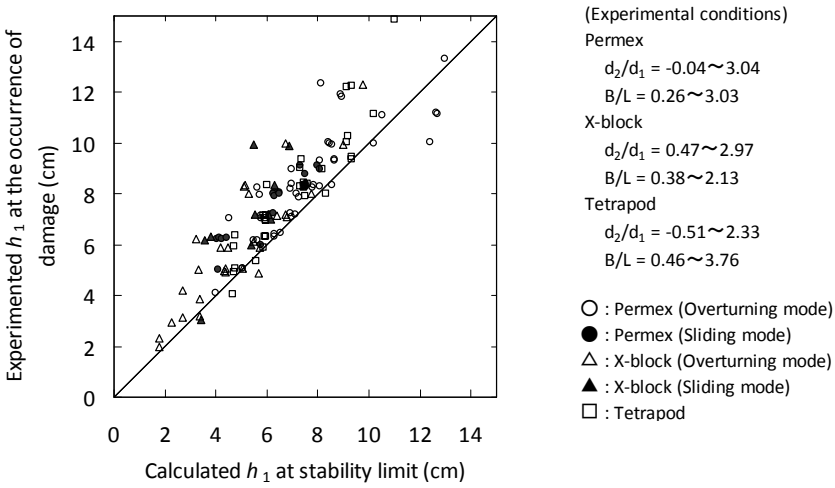

Figure 14: Calculated and Experimented Overflow Depth h_1 of the Stability Limit

3. NEW TECHNOLOGY FOR LONG-PERIOD WAVE ABSORPTION USING CONCRETE BLOCKS

3.1 Experimental Setup

The fundamental properties in the wave absorbing performance of the conventional and newly developed submerged type long-wave absorbing structures were examined by hydraulic model experiments. A series of experiments was conducted using a 50 m-long, 1.0 m-wide and 1.3 m-deep wave flume equipped with a piston type wave generator. Fig. 15 shows the test setup in the flume. The long-period wave absorbing structure model was situated on a horizontal bottom modeling a uniform depth in the harbor. The wave reflection coefficient K_R was estimated based on Goda and Suzuki (1976) using instantaneous records of water surface elevation obtained by two wave gauges located at the center of the horizontal bottom keeping the gauge spacing one-fourth of a wavelength. Since monochromatic waves corresponding to the resonance frequency of the harbor are an important factor, regular waves with periods of 4.24 to 16.97 s and heights of 0.5 to 3.0 cm were used. The model scale was set to 1/50 based on the Froude number.

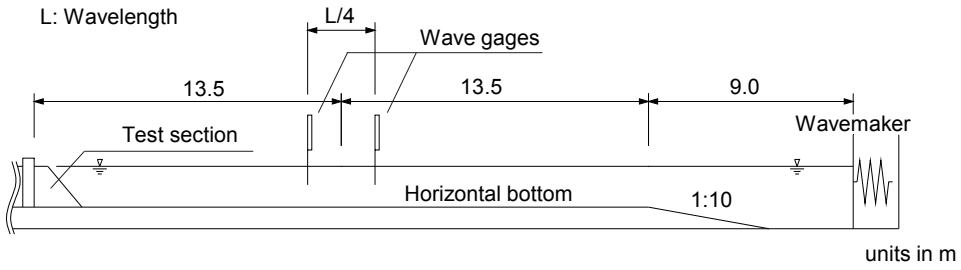

Figure 15: Test Setup in the Flume

In the initial stage, fundamental properties in wave absorbing performance of conventional and submerged type were investigated. After this, the characteristics of the submerged type were analyzed in detail. The test sections in the initial stage are shown in Fig. 16. The crown heights above the water level for the conventional type were set to 10.0 cm. On the other hand, the crest elevation of the submerged type coincided with the water level.

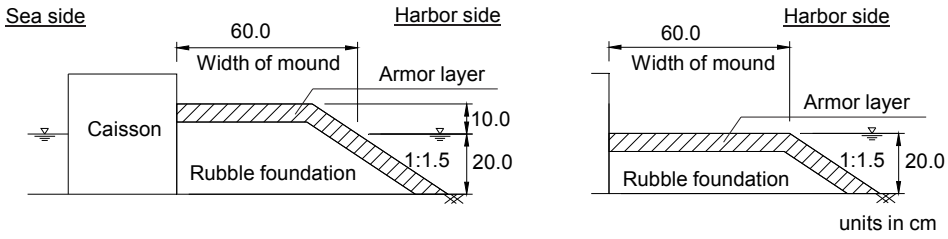

(a) Conventional Type **(b) Submerged Type**

Figure 16: Test Sections for Wave Absorbing Properties

The experimental conditions are shown in Table 1. The rubble foundation consisted of 0.4 to 1.6 g stones. In the initial stage, the water depth was 20.0 cm. The width was set to 60.0 cm. Armor stones were used because the conventional type structures had been installed with armor stones on site. In the second stage, the water depth was 14.0 to 32.0 cm. The widths were set to 30.0 cm or 60.0 cm. Tetrapod and X-block were used as examples of concrete blocks. Fig. 17 shows the geometry of the blocks.

Table 1: Test Conditions for Wave Absorbing Properties

	Model		Prototype	
Scale	1/50		1	
Wave period	4.24 – 16.97s		30 – 120s	
Wave height	0.5 – 3.0cm		0.25 – 1.50m	
Crown height above the water level	Conventional: 10cm Submerged: 0cm		Conventional: 5m Submerged: 0m	
Rubble foundation	0.4 – 1.6g		50 – 200kg	
Mound slope	1:1.5		1:1.5	
Water depth	Initial stage	Second stage	Initial stage	Second stage
	20cm	14, 20, 26 and 32cm	10m	7, 10, 13 and 16m
Width of mound	60cm	30 and 60cm	30m	15 and 30m
Armor material	8.0g armor stones (two-layer)	14.5g, 60.5g, 121.0g, 235.1g Tetrapods (two-layer) 16.2g X-Blocks	1t armor stones (two-layer)	2t, 8t, 15t, 29t Tetrapods (two-layer) 2t X-Blocks

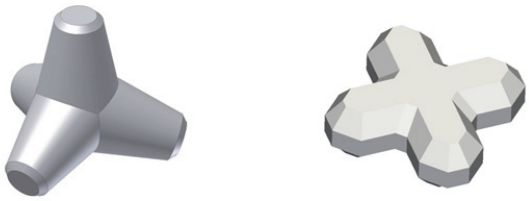

Tetrapod X-block

Figure 17: Concrete Blocks Used in the Experiment

3.2 Influence of Crown Height

Hereafter a prototype scale notation is used unless a particular explanation is given. Fig. 18 compares the reflection coefficients of the conventional and submerged type shown in Fig. 16. Both structures are covered with armor stones and of width at the still water level of 30 m. The reflection coefficient of the submerged type is smaller than that of conventional type independent of the wave period. As is often pointed out in the literature, for example Madsen (1983), the energy dissipation of a permeable breakwater takes place not only inside the porous structure but also on the surface of the structure due to friction. Since the submerged type has a larger amount of surface area compared to that of the conventional type, it is thought that the surface area of submerged type leads to effective energy dissipation due to the friction there. In the rest of this paper, the submerged type is mainly focused on.

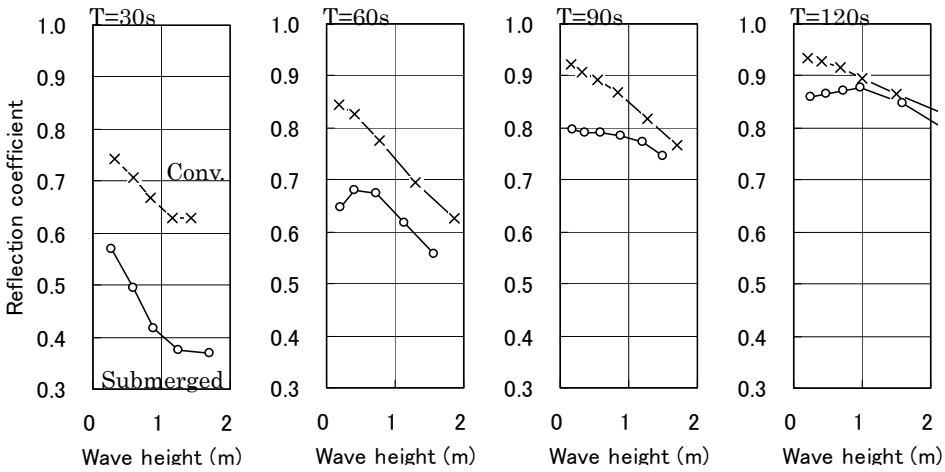

Figure 18: Reflection Coefficients of Conventional Type and Submerged Type

3.3 Influence of Armor Material

Fig. 19 shows the relationship between the wave period and the reflection coefficients of the submerged type with various armor materials, i.e., armor stones, Tetrapod and X-block. When the wave period is below 80 s, the K_R with Tetrapod covering is the smallest among all the structures, while that with the armor stone covering is the smallest against wave periods above 80 s. The K_R with Tetrapod covering seems to converge to 0.9 within the range of this study. The change in K_R with X-block covering with variation in the wave period is almost the same as that with armor stone covering. Although the details are not shown, a non-significance in the dependency of the size of the Tetrapod on K_R was observed. Because the Tetrapod covered mound can realize low wave reflection in a wide range of wave periods, the use of Tetrapod is effective for this structure.

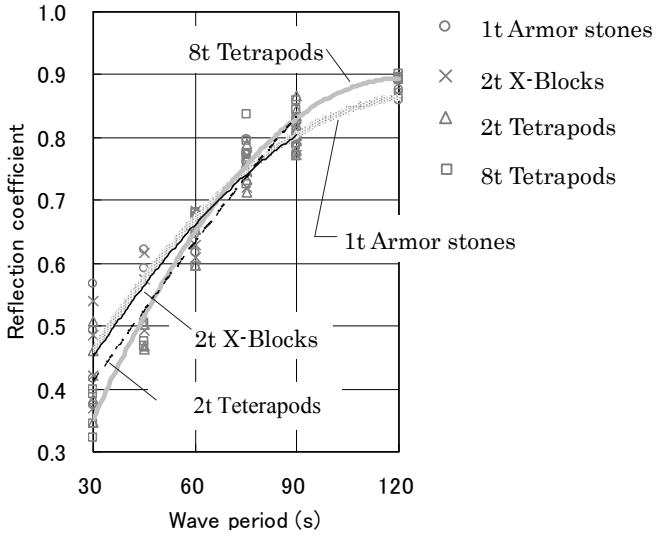

Figure 19: Relationship between Wave Period and K_R

3.4 Influence of Water Level Change

In the previous subsection, the usefulness of submerged mound type structure was clearly confirmed. The high wave absorbing performance for idealized conditions, i.e., the crest elevation coincided with the water level was well verified. However, in an actual site condition, the structure would be exposed to water level variation. Accordingly, in the following, the influence of water level change is discussed. In the coasts around Japan, the difference between flood and ebb tide is less than 2.5 m with a few exceptions. Therefore in our experiments, a tidal variation of ± 1.5 m was provided by changing the water depth from 8.5 to 11.5 m against the fixed mound geometries as shown in Fig. 16. In our experiments, 1 t armor stones or 8 t tetrapod was used for the conventional and submerged type as armor material. Fig. 20 shows the relationship between the water depth h and the wave reflection coefficient K_R under the condition where the wave height is 0.5 m. It is known that a long-period wave with wave height below 0.5 m caused decrease in the efficiency of cargo handling as shown in Hiraishi et al. (1996). The reflection coefficients of the conventional type increase with increase in water depth. On the other hand, those of the submerged type show a V-shaped distribution with a minimum value at the water depth of 10m, the idealized condition mentioned above. Although K_R increases when the water level varies from its idealized position, the K_R of the submerged type indicates smaller values than those of the conventional type within the tidal range of ± 1.0 m. This confirms the robustness of the submerged type with Tetrapod covering.

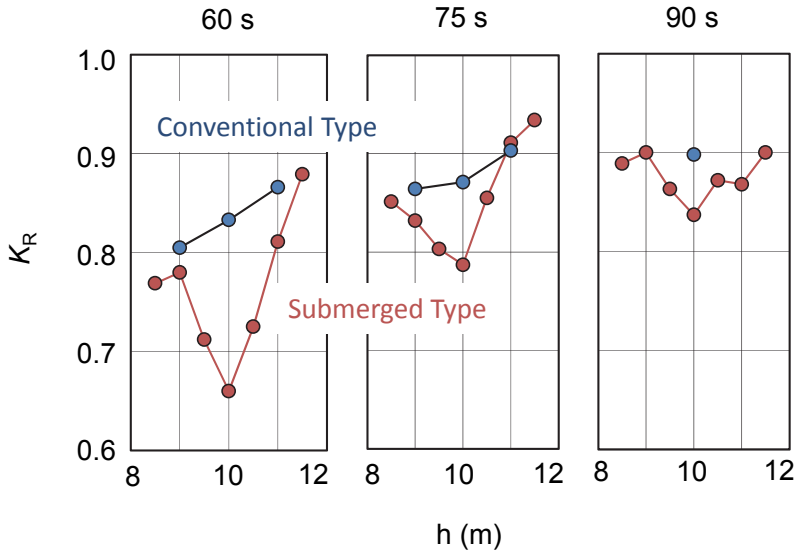

Figure 20: Relationship between Water depth and K_R

3.5 Wave Absorbing Mechanism

In the previous section, the usefulness of the submerged type was clearly confirmed. In this section, the wave absorbing mechanism is discussed through numerical analysis and hydraulic model experiments. A multiphase flow solver using the VOF method within the OpenFOAM CFD model (OpenFOAM foundation, 2011) was applied to the analysis. The hydraulic flow resistance R in the porous medium was expressed by a Dupuit-Forchheimer low (Forchheimer, 1901) as follows:

$$R = -\left(\alpha U + \beta |U| U\right) \tag{13}$$

where, U is the velocity vector, α is the laminar resistance coefficient and β is the turbulent resistance coefficient. These coefficients are expressed in the empirical formulae by Engelund (1953) as follows:

$$\alpha = \alpha_0 \frac{(1-\gamma)^3}{\gamma^2} \frac{\nu}{d^2} \quad , \quad \beta = \beta_0 \frac{1-\gamma}{\gamma^3} \frac{1}{d} \tag{14}$$

where, v is the kinematic viscosity of water, d is a nominal diameter of the stone, γ is the porosity, and α_0 and β_0 are the material constants. Although it is omitted here, the α_0 and β_0 were examined in advance in this study.

Fig. 21 shows the wave flume setup for computation. Long-period waves were made by oscillatory flow on a horizontal bottom of the wave flume. The wave energy dissipating unit was arranged in the opposite side of the mound structure model. The other computational conditions were the same as the experimental ones. Fig. 22 compares the wave reflection coefficient K_R of the mounds obtained by numerical analysis and by the experiments. Both mounds are covered with the armour stones. The computation reproduces the experimental value well. The validity of this analysis method was confirmed.

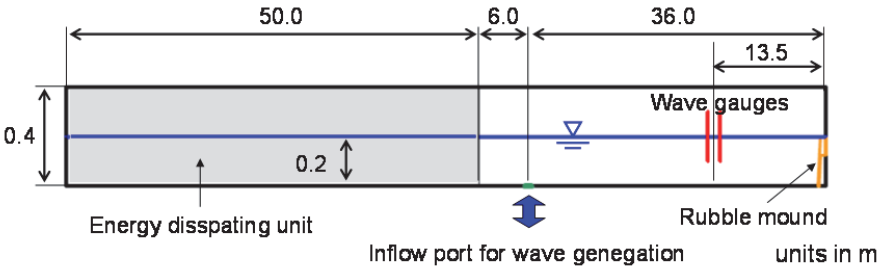

Figure 21: Wave Flume Setup for Computation

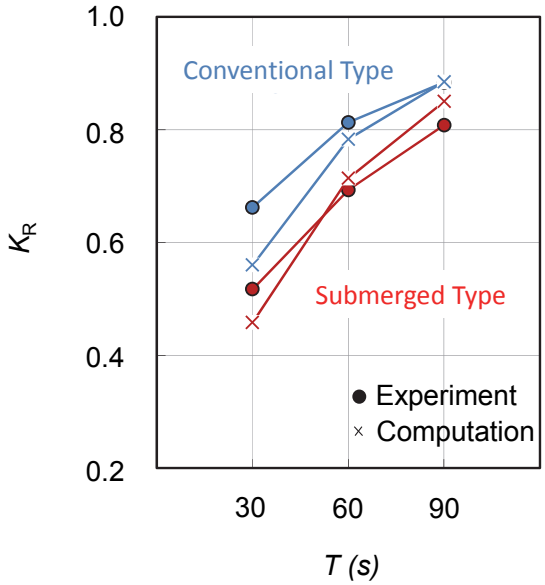

Figure 22: Comparison of Computation with Experiment

Energy breakdown was verified in the process of wave reflection on both mounds, for the purpose of looking into the wave absorbing factor. The incident wave energy flux is expressed as follows:

$$E_I C_G = \frac{1}{8}\rho g H_I^2 C_G \tag{15}$$

where, E_I is the incident wave energy, C_G is the group velocity, ρ is the density of the water and H_I is the incident wave height at the center of the two wave gauges. This energy flux $E_I C_G$ is balanced to the total energy flux of the energy dissipating flux E_D and the reflected wave energy flux E_R calculated as K_R^2. Furthermore, the E_D can be parted a dissipated energy ratio E_{Res} by the fluid resistance generated in passing through the porous structure and a remaining dissipated energy ratio E_{Etc} due to others like sea bottom and surfaces or gaps of caissons. The E_{Res} can be calculated from the value of 1 cycle average of the absorbed energy due to the mound units per unit time. Equation (15) shows the absorbed energy per unit time P:

$$P = \int_S \rho R \cdot U dS \tag{16}$$

Fig. 23 shows the wave energy balance in each type with armour stones shown in Fig. 16. The rate of the total energy flux is expressed as 1.0 by dividing by the incident wave energy flux $E_I C_G$. As shown in this figure, the same tendencies with experimental results were obtained. The value of E_R increases with increase in wave period. The value of E_R of the submerged type is smaller than that of the conventional type independent of wave period. As for the energy dissipating flux E_D, E_{Etc} is almost constant regardless of the calculation condition. This result suggests that the energy dissipation due to the mound by fluid resistance is predominant for a long-period wave absorption.

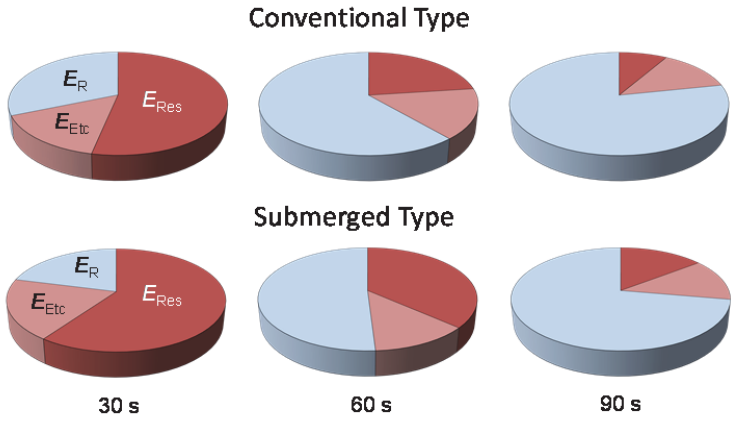

Figure 23: Wave Energy Balance in Conventional Type and Submerged Type

Since the submerged type has a larger amount of surface area in the vicinity of the water surface compared to that of the conventional type, it is expected that the surface area of the submerged type leads to effective energy dissipation. Accordingly, K_R of the mounds with impermeable rubble foundation was examined to investigate the effect of the material in armor layer for the energy dissipation. Total energy dissipating flux of the impermeable foundation $E_{D\text{-}imp}$ and E_D of the submerged type are expressed as follows:

$$E_{D-imp} \approx E_{Res-imp} = E_{C-imp} + E_{S-imp} \tag{17}$$

$$E_D \approx E_{Res} = E_C + E_S + E_F \tag{18}$$

where, E_C is the energy dissipation at the crown of the armor layer by the fluid resistance, E_S is that at the slope of the armor layer and E_F is that in the rubble foundation as show in Fig. 24. The figure shows the rate of change r_{imp} of the $E_{D\text{-}imp}$ to that of the E_D, with Tetrapod armor, calculated as $1\text{-}K^2_R$ by the experiment respectively. Although, the r_{imp} of the conventional type decreased in 27 to 40 %, the r_{imp} of the submerged type increased in 3 to 19 % in range of the wave period of 60 to 90 s. It is thought that the energy dissipation of the submerged type mainly occurred at the armor layer since the $E_{D\text{-}imp}$ was larger than E_D without any effect of the E_F. That is, it can be thought that the cause of the effective energy dissipation of the submerged type is related to a significant increase in the flow velocity inside the armor layer due to the flow contraction onto the crest.

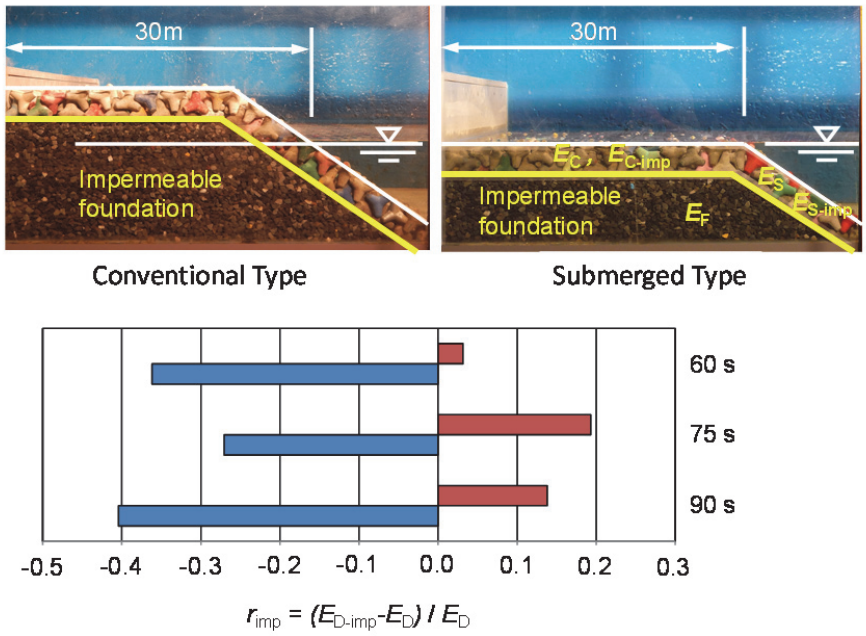

Figure 24: Rate of Change of Wave Energy Dissipation

3.6 Structure Width Estimation Method

Fig. 25 shows the relationship between the equivalent mound width normalized by the wavelength B^*/L and the reflection coefficient K_R of the submerged type with 8t Tetrapod armor layer for various combinations of water depths and widths of the mound. A definition of B^* is found in the figure. Because water particle motion of long-period waves is still present even near the sea bottom, the use of B*, which includes the influence of water depth, is more appropriate when compared to the simple crown width B which is used for the current design of conventional type. It can be seen that K_R can be estimated by using B*/L independently of the water depth and width of the mound.

By using this diagram, the required widths of structure were obtained under specified reflection coefficients, water depths, wave periods and slopes of the structure. For example, a 16.8 m width was calculated for the submerged type with tetrapods while a 32.8 m width was obtained for the conventional structure with armor stones if the required reflection coefficient was 0.85, the water depth was 10 m, the wave period was 60 s and the slope of structure was 1:1.5. Table 2 summarizes the details of the derivation.

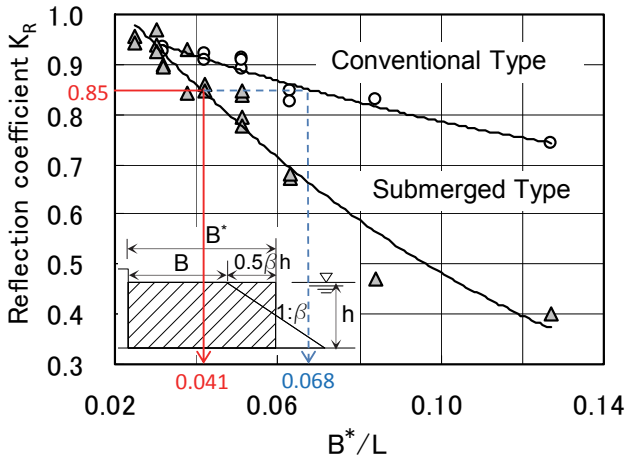

Figure 25: Design Diagram of Required Mound Width

Table 2: Comparison of Structural Width between Conventional Type and Submerged Type

K_R	Slope	h (m)	T (s)	L (m)	B^*/L		B^* (m)		B (m)	
					Submerged	Conv.	Submerged	Conv.	Submerged	Conv.
0.85	1:1.5	10.0	60.0	593	0.041	0.068	24.3	40.3	16.8	32.8

3.7 Experience of Construction

In Kashima Port located northeast of Tokyo, the submerged type structure with concrete blocks was constructed for a countermeasure against long-period waves. Kashima Port, an artificially excavated industrial port, was constructed on a sand beach of total length of about 70 km (Kashima-Nada) which faces the Pacific Ocean. Fig. 26 shows the location. Breakwaters have been extended in order to reduce the energy of the long-period waves from the sea. A submerged type structure has been installed behind the breakwater.

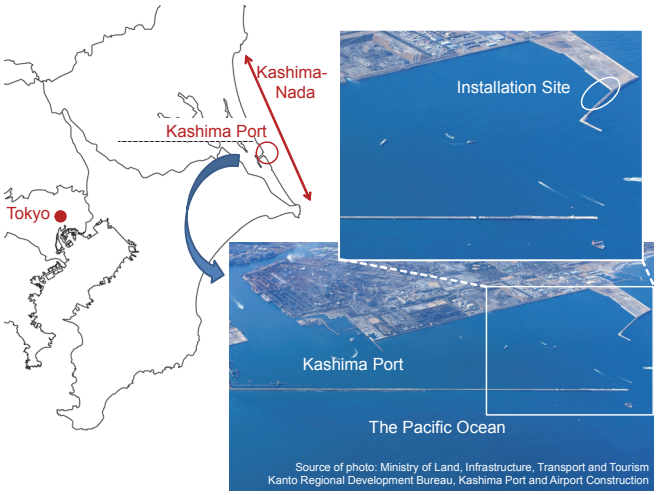

Figure 26: Installation Site of Submerged Type Structure (Kashima Port)

4. Conclusions

A practical design method with concrete blocks to cover a widened protection at the rear of a caisson breakwater against tsunami overflow has been proposed. The features of this method are summarized as follows:

- The overflow depth is used to represent the external force. This enables the estimation of the required mass of the concrete blocks to be done more robustly and easily than in the conventional method based on flow velocity.
- Two formulae are used corresponding to the two failure modes, overturning and sliding.
- This method takes into account the influence of the impingement position of an overflow jet and the influence of the harbor-side water depth. These factors are important for block stability.
- The stability numbers N_{S1} and N_{S2} for each armor unit were determined through experiments conducted in a wide range of conditions. The estimated results by this method agreed well with the experimental ones.

As a countermeasure to problems in cargo handling, a submerged type long-period wave absorbing structure has been developed. The features of this newly proposed structure are summarized as follows:

- The submerged type is more effective than the conventional type on dissipating long-period waves. As a result, the cost and space of the wave absorbing structure can be improved.
- The predominant factor for the energy dissipation of the long-period waves was the dissipated energy flux due to the armor units by the fluid resistance. It is also thought that the cause of the effective dissipation of the submerged type is related to a significant increase in the flow velocity inside the armor layer due to flow contraction on to the crest.
- It is possible to design an appropriate width of submerged type in general breakwater conditions by using the proposed design diagram.

References

Arikawa, T., M. Sato, K. Shimosako, T. Tomita, G. Yeom, and T. Niwa. (2013). Failure mechanism and resiliency of breakwaters under tsunami, Technical Note of the Port and Airport Research Institute, No. 1269 (in Japanese).

Coastal Engineering Research Center. (1977). Shore Protection Manual, U.S. Army Corps of Engineers, U.S. Government Printing Office, Vol. II, 7_213-7_216.

Engelund, F. (1953). On the laminar and turbulent flows of ground water through homogeneous sand, Transactions of the Danish Academy of Technical Sciences, Vol. 3, No. 4.

Forchheimer P. (1901). Wasserbewegung durch Boden, Zeit. Ver. Deut. Ing., Vol 45, pp 1781-1788.

Goda, Y. and Suzuki, Y. (1976). Estimation of incident and reflected waves in random wave experiments. Proc. 15th International Conference on Coastal Engineering, Honolulu, Vol.1, pp.828-845.

Hamaguchi, M., S. Kubota, A. Matsumoto, M. Hanzawa, M. Yamamoto, H. Moritaka, and K. Shimosako. (2007). Hydraulic stability of new flat type armor block with very large openings for use in composite breakwater rubble mound protection, Proceedings of Coastal Structures 2007, ASCE, 116-127.

Hiraishi, T., Tadokoro, A. and Fujisaku, H. (1996). Characteristics of Long Period Wave Observed in Port, Report of the Port and Harbour Research Institute, Vol.35, No.3, pp.3-36. (in Japanese)

Hom-ma, M. (1940a). Discharge coefficient on overflow weir (part-1), JSCE Magazine, Civil Engineering, Vol. 26, No. 6, 635-645 (in Japanese).

Hom-ma, M. (1940b). Discharge coefficient on overflow weir (part-2), JSCE Magazine, Civil Engineering, Vol. 26, No. 9, 849-862 (in Japanese).

Kubota, S., M. Hamaguchi, A. Matsumoto, M. Hanzawa, and M. Yamamoto. (2008). Wave force and stability of new flat type concrete block with large openings for submerged breakwaters, Proceedings of 31st International Conference on Coastal Engineering, ASCE, 3423-3435.

Madsen, P. A. (1983) Wave Reflection from a Vertical Permeable Wave Absorber. Coastal Engineering, Vol.7, pp.381-396.

Ministry of Land, Infrastructure, Transport and Tourism, Port and Harbor Bureau. (2013). Design guideline of breakwaters against tsunami (in Japanese).

OpenFOAM foundation Ltd. (2011). OpenFOAM User Guide version 2.0.1, http://www.openfoam.org

Van der Meer, J.W. (1988). Stability of cubes, tetrapods and accropode, Proceedings of Conf. Breakwaters ’88, 71-80.